

Measurement of Strange Quark Contributions to the Nucleon's Form Factors at $Q^2=0.230$ (GeV/c)²

F. E. Maas,^{1,*} P. Achenbach,¹ K. Aulenbacher,¹ S. Baunack,¹ L. Capozza,¹ J. Diefenbach,¹ K. Grimm,¹ Y. Imai,¹ T. Hammel,¹ D. von Harrach,¹ E.-M. Kabuß,¹ R. Kothe,¹ J. H. Lee,¹ A. Lorente,¹ A. Lopes Ginja,¹ L. Nungesser,¹ E. Schilling,¹ G. Stephan,¹ C. Weinrich,¹ I. Altarev,² J. Arvieux,³ B. Collin,³ R. Frascaria,³ M. Guidal,³ R. Kunne,³ D. Marchand,³ M. Morlet,³ S. Ong,³ J. van de Wiele,³ S. Kowalski,⁴ B. Plaster,⁴ R. Suleiman,⁴ and S. Taylor⁴

¹*Institut für Kernphysik, Johannes Gutenberg Universität Mainz, J. J. Becherweg 45, D-55099 Mainz, Germany*

²*St. Petersburg Institute of Nuclear Physics, Gatchina, Russia*

³*Institut de Physique Nucleaire, 91406 - Orsay Cedex, France*

⁴*Laboratory for Nuclear Science, Massachusetts Institute of Technology, Cambridge, MA 02139, USA*

(Dated: August 7, 2018)

We report on a measurement of the parity-violating asymmetry in the scattering of longitudinally polarized electrons on unpolarized protons at a Q^2 of 0.230 (GeV/c)² and a scattering angle of $\theta_e = 30^\circ - 40^\circ$. Using a large acceptance fast PbF₂ calorimeter with a solid angle of $\Delta\Omega = 0.62$ sr the A4 experiment is the first parity violation experiment to count individual scattering events. The measured asymmetry is $A_{\text{phys}} = (-5.44 \pm 0.54_{\text{stat}} \pm 0.26_{\text{sys}}) \times 10^{-6}$. The Standard Model expectation assuming no strangeness contributions to the vector form factors is $A_0 = (-6.30 \pm 0.43) \times 10^{-6}$. The difference is a direct measurement of the strangeness contribution to the vector form factors of the proton. The extracted value is $G_E^s + 0.225G_M^s = 0.039 \pm 0.034$ or $F_1^s + 0.130F_2^s = 0.032 \pm 0.028$.

PACS numbers: 12.15.-y, 11.30.Er, 13.40.Gp, 13.60.Fz, 14.20.Dh

The understanding of sea-quark degrees of freedom of the nucleon and the interaction of the quarks with the vacuum in the nonperturbative low energy regime of quantum chromodynamics (QCD) is very poor even today. Since the nucleon has no net strangeness, any contribution of strange quarks to the nucleon structure observables is of particular interest because it would be a pure sea-quark effect. For example the scalar strangeness content of the nucleon that gives a contribution to the mass of the nucleon has been discussed in the context of the Σ commutator which can be related to the π -N scattering amplitude [1]. New measurements suggest a large contribution of strange quarks to the mass of the nucleon on the order of 50%. The interpretation of the unexpected nucleon spin content results [2] suggests a sizeable contribution, $\Delta s \approx -10\%$, of the strange quarks to the nucleon spin. Estimates of the strange quark contribution to the magnetic and electric vector form factors predict sizeable effects accessible to experiments [3, 4]. Recently, two experiments, SAMPLE at Bates [5] and HAPPEX at TJNAF [6], have explored parity-violating (PV) asymmetries on the proton and the deuteron in two different kinematical regions. We report here on a new measurement at a four momentum transfer Q^2 of 0.230 (GeV/c)² at the Mainzer Mikrotron accelerator facility (MAMI) [7]. The A4 experiment at MAMI is complementary to other experiments for two reasons. Firstly its Q^2 -value tests models predicting an enhanced strangeness contribution at this point [8] and secondly, for the first time counting techniques are used in a scattering experiment measuring a PV asymmetry. Therefore possible systematic contributions to the experimental asymmetries and the associated uncertainties are of a different nature as compared to previous experiments, which use analogue integrating techniques. Access to the strangeness nucleon vector current matrix elements is possible in the framework of the standard model

by a measurement of the weak vector form factors $\tilde{G}_{E,M}^p$ of the proton [9]. They can be expressed in terms of the known nucleon electro-magnetic vector form factors $G_{E,M}^{p,n}$ and the unknown strangeness contribution $G_{E,M}^s$. The interference between weak (Z^0) and electro-magnetic (γ) amplitudes leads to a PV asymmetry $A_{LR}(\vec{e}p)$ in the elastic scattering cross section for right- and left-handed electrons (σ_R and σ_L respectively), which is given in the framework of the Standard Model [10] and can be expressed as a sum of three terms, $A_{LR}(\vec{e}p) = A_V + A_s + A_A$, with

$$A_V = -a \rho'_{eq} \left\{ (1 - 4\hat{\kappa}'_{eq}\hat{s}_Z^2) - \frac{\varepsilon G_E^p G_E^n + \tau G_M^p G_M^n}{\varepsilon(G_E^p)^2 + \tau(G_M^p)^2} \right\}, \quad (1)$$

$$A_s = a \left\{ \rho'_{eq} \frac{\varepsilon G_E^p G_E^s + \tau G_M^p G_M^s}{\varepsilon(G_E^p)^2 + \tau(G_M^p)^2} \right\}, \quad (2)$$

$$A_A = a \left\{ \frac{(1 - 4\hat{s}_Z^2) \sqrt{1 - \varepsilon^2} \sqrt{\tau(1 + \tau)} G_M^p \tilde{G}_A^p}{\varepsilon(G_E^p)^2 + \tau(G_M^p)^2} \right\}. \quad (3)$$

A_V represents the vector coupling on the proton vertex where the possible strangeness contribution has been taken out and has been put into A_s . A_s is a term arising only if a contribution from strangeness to the electro-magnetic vector form factors is present and the term A_A represents the contribution from the axial coupling at the proton vertex due to the neutral current weak axial form factor \tilde{G}_A^p . The quantity a represents $(G_\mu Q^2)/(4\pi\alpha\sqrt{2})$. G_μ is the Fermi coupling constant as derived from muon decay. α is the fine structure constant, Q^2 the negative square of the four momentum transfer, $\tau = Q^2/(4M_p^2)$ with M_p the proton mass and $\varepsilon = [1 + 2(1 + \tau)\tan^2(\theta_e/2)]^{-1}$ with θ_e the laboratory scattering angle of the electron. The electro-magnetic form factors $G_{E,M}^{p,n}$ are taken from a recent parametrization (version 1, page 5) by Friedrich and Walcher [11], where we assign an experimental error of 3% to G_M^p and

G_E^p , of 5% to G_M^n , and of 10% to G_E^n . Electro-weak radiative corrections are included in the factors ρ'_{eq} and k'_{eq} which have been evaluated in the \overline{MS} renormalization scheme [12]. We use a value for $\hat{s}_Z^2 = \sin^2 \hat{\theta}_W(M_Z)_{\overline{MS}}$ of 0.23113(15) [13]. The electro-weak radiative corrections to A_A have also been estimated within the \overline{MS} renormalization scheme and the radiative corrections given in [14] as well as a value of $\Delta s = -0.1 \pm 0.1$ are included in \hat{G}_A . Electro-magnetic internal and external radiative corrections to the asymmetry and the effect of energy loss due to ionization in the target have been calculated. They reduce the expected asymmetry in our kinematics by about 1.3%. In order to compare to the measured asymmetry, we include the effects of electro-magnetic radiative corrections and energy loss in the target and average $A_0 = A_V + A_A$ over the acceptance of the detector and the target length. We obtain the expected value for the asymmetry at the averaged Q^2 without strangeness contribution to the vector form factors of $A_0(Q^2 = 0.230(\text{GeV}/c)^2) = -6.30 \pm 0.43$ ppm.

The PV asymmetry was measured at the MAMI accelerator facility in Mainz [7] using the setup of the A4 experiment [15]. The polarized 854.3 MeV electrons were produced using a strained layer GaAs crystal which is illuminated with circularly polarized laser light [16]. Average beam polarization was about 80%. The helicity of the electron beam has been selected every 20.08 ms by setting the high voltage of a fast Pockels cell according to a pattern of four helicity states, either $(+P - P - P + P)$ or $(-P + P + P - P)$. The pattern was selected randomly by a pseudo-random bit generator. A 20 ms time window enabled the histogramming in all detector channels and an integration circuit in the beam monitoring and luminosity monitoring systems. The exact window length was locked to the power frequency of 50 Hz in the laboratory by a phase locked loop. For normalization, the gate length was measured for each helicity. Between each 20 ms measurement gate, there was an 80 μs time window for the high voltage at the Pockels cell to be changed. The intensity $I = 20 \mu\text{A}$ of the electron current was stabilized to better than $\delta I/I \approx 10^{-3}$. An additional $\lambda/2$ -plate in the optical system was used to rotate small remaining linear polarization components and to control the helicity correlated asymmetry in the electron beam current to the level of < 10 ppm in each five min run.

We have used a system of microwave resonators in order to monitor beam current, energy, and position in two sets of monitors separated by a drift space of about 7.21 m in front of the hydrogen target. In addition, we have used a system of 10 feed-back loops in order to stabilize current, energy [17], position, and angle of the beam. The polarization of the electron beam was measured using a Møller polarimeter which is located on a beam line in another experimental hall. This Møller polarimeter [18] has an accuracy of 2.1%. Due to the fact, that we have to interpolate between the weekly Møller measurements, the uncertainty in the knowledge of the beam polarization increased to 4%. The 10 cm high power, high flow liquid hydrogen target was optimized to guarantee a high degree of turbulence with a Reynolds-number of $R > 2 \times 10^5$ in the target cell in order to increase the effective heat trans-

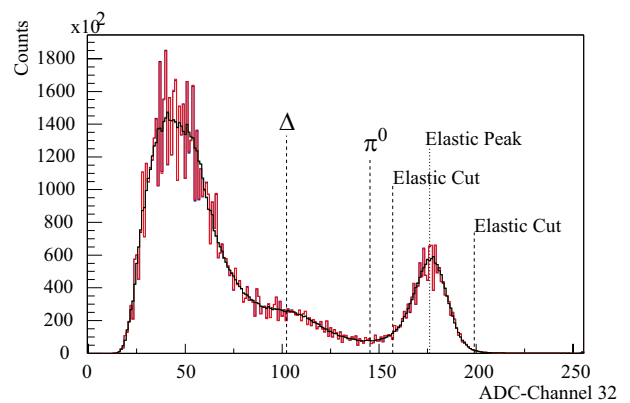


FIG. 1: An energy spectrum of accepted particles from the hydrogen target as read directly from the hardware memory of the read out electronics of the lead fluoride calorimeter. For the solid black curve, the spectrum has been corrected for the differential nonlinearity of the ADC. The position of the elastic scattering peak, the threshold for π^0 -production and the position of the Δ -resonance is indicated as well as the lower and upper cut position for the extraction of N_e^R and N_e^L as described in the text.

fer. This new technique allowed us for the first time to avoid a fast modulation of the beam position of the intense cw 20 μA beam and it also allowed us to stabilize the beam position on the target cell without target density fluctuations arising from boiling. The total thickness of the entrance and exit aluminum windows is 250 μm . The luminosity L was monitored for each helicity state (R, L) during the experiment using eight water-Cerenkov detectors (LuMo) that detect scattered particles symmetrically around the electron beam for small scattering angles in the range of $\theta_e = 4^\circ - 10^\circ$, where the PV asymmetry is negligible. The photomultiplier tube currents of these luminosity detectors are integrated during the 20 ms measurement period by gated integrators and then digitized by customized 16-bit analogue-to-digital converters (ADC). The same method was used for all the beam parameter signals and these data were stored with the helicity information as a function of time for each 20 ms time window. A correction was applied for the nonlinearity of the luminosity monitor photomultiplier tubes. This was measured and verified separately by varying the beam current from 0-23 μA several times per week. From the beam current helicity pair data $I^{R,L}$ and luminosity monitor helicity pair $L^{R,L}$ data we calculated the target density $\rho^{R,L} = L^{R,L}/I^{R,L}$ for the two helicity states independently for the analysis of the data.

As particle detector we developed a new type of a very fast, homogeneous, total absorption calorimeter consisting of individual lead fluoride (PbF_2) crystals [19]. The material is a pure Cerenkov radiator and has been chosen for its fast timing characteristics and its radiation hardness [20]. This is the first time this material is used in a large scale calorimeter for a physics experiment. The crystals are dimensioned so that an electron deposits 96% of its total energy in an electro-

magnetic shower extending over a matrix of 3×3 crystals. Together with the readout electronics this allows us a measurement of the particle energy with a resolution of $3.9\%/\sqrt{E}$ and a total dead time of 20 ns. At the time of the data taking, 511 channels of the detector and the read out electronics were operational. The detector modules were located in two sectors covering an azimuthal angle interval $\Delta\phi$ of 90° symmetrically around the beam axis. The particle rate within the acceptance of this solid angle is $\approx 50 \times 10^6 \text{ s}^{-1}$. Due to the short dead time, the losses due to double hits in the calorimeter are 1% at $20 \mu\text{A}$. The signals from each cluster of 9 crystals are summed and integrated for 20 ns in an analogue summing and triggering circuit and digitized by a transient 8-bit ADC. There is one summation, triggering, and digitization circuit per crystal. The energy, helicity, and impact information are stored together in a three dimensional histogram. Figure 1 shows a typical energy spectrum of scattered particles from the hydrogen target at an electron current of $20 \mu\text{A}$. It was taken during five minutes and is a direct output of the histogramming memory. The elastic scattering peak is clearly isolated at the high end of the spectrum.

The energy resolution σ_E of each group of 9 crystals was determined by analyzing such spectra. The number of elastic scattered electrons is determined for each detector channel by integrating the number of events in an interval from $1.6 \sigma_E$ above pion production threshold to $2.0 \sigma_E$ above the elastic peak in each helicity histogram. The usage of those cuts ensures a clean separation between elastic scattering and pion production or Δ -excitation which has an unknown PV cross section asymmetry. We determined the number of elastically scattered electrons for each helicity state (N_e^R and N_e^L) by summing over the inner 345 detector channels which are the centers of a full 3×3 crystal matrix. The linearity of the PbF_2 detector system with respect to particle counting rates and possible effects due to dead time were investigated by varying the beam current. We calculate the raw normalized detector asymmetry as $A_{\text{raw}} = (N_e^R/\rho^R - N_e^L/\rho^L)/(N_e^R/\rho^R + N_e^L/\rho^L)$. The possible dilution of the measured asymmetry by background originating from the production of π^0 which subsequently decays into two photons where one of the photons carries almost the full energy of an elastic scattered electron was estimated using Monte Carlo simulations to be much less than 1% and is neglected here. The largest background comes from quasi elastic scattering at the thin aluminum entrance and exit windows of the target cell. We have measured the aluminum quasielastic event rate and calculated in static approximation a correction factor for the aluminum of 1.030 ± 0.003 giving a smaller value for the corrected asymmetry.

Corrections to false asymmetries arising from helicity correlated changes of beam parameters were applied on a run by run base. The analysis was based on the five min runs for which the counted elastic events in the PbF_2 detector were combined with the correlated beam parameter and luminosity measurements. In the analysis we applied reasonable cuts in order to exclude runs where the accelerator or parts of the PbF_2 detector system were malfunctioning. The analysis is

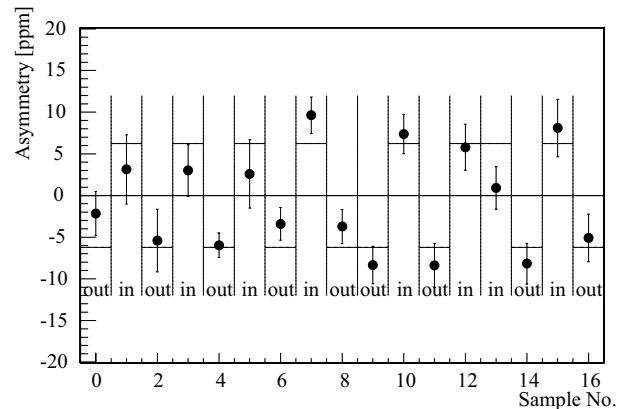


FIG. 2: The extracted experimental asymmetries are shown with $\lambda/2$ -plate in or out respectively as a function of the data sample. The dashed line represents the value of A_0 as described in the text.

based on a total of 7.3×10^6 histograms corresponding to 4.8×10^{12} elastic scattering events.

We extracted an experimental asymmetry from $A_{\text{exp}} = A_{\text{raw}} - a_1 A_I - a_2 \Delta x - a_3 \Delta y - a_4 \Delta x' - a_5 \Delta y' - a_6 \Delta E_e$. The six a_i ($i = 1 \dots 6$) denote the correlation coefficients between the observed false asymmetry and the electron current asymmetry A_I (a_1), the horizontal and vertical beam position differences Δx , Δy (a_2 , a_3), the horizontal and vertical beam angle differences $\Delta x'$, $\Delta y'$ (a_4 , a_5), and the beam energy difference ΔE_e (a_6). For the analysis, the correlation parameters a_i were extracted by multidimensional regression analysis from the data. The a_i have been calculated in addition from the geometry of the precisely surveyed detector geometry and the a_i calculated using the two different methods agree very well within statistics.

The experimental asymmetry was normalized to the electron beam polarization P_e to extract the physics asymmetry, $A_{\text{phys}} = A_{\text{exp}}/P_e$. We have taken half of our data with a second $\lambda/2$ -plate inserted between the laser system and the GaAs crystal. This reverses the polarization of the electron beam and allows a stringent test of the understanding of systematic effects. The effect of the plate can be seen in Fig. 2: the observed asymmetry extracted from the different data samples changes sign, which is a clear sign of parity violation if, as in our case, the target is unpolarized. Our measured result for the PV physics asymmetry in the scattering cross section of polarized electrons on unpolarized protons at an average Q^2 value of $0.230 (\text{GeV}/c)^2$ is $A_{\text{phys}} = (-5.44 \pm 0.54 \pm 0.26)$ ppm. The first error represents the statistical accuracy, the second error the systematical uncertainties including beam polarization. The absolute accuracy of the experiment represents the most accurate measurement of a PV asymmetry in the elastic scattering of longitudinally polarized electrons on unpolarized protons. Table I gives an overview of the applied corrections and the contributions to the systematical error of the experimental asymmetry.

The interpretation of the measurement in terms of strangeness

TABLE I: Overview of the applied corrections and the sources of the experimental error in the measured asymmetry.

	correction [ppm]	error [ppm]
Statistics		0.54
Target density, luminosity	0.58	0.09
Target density, beam current	0.00	0.04
Nonlinearity of LuMo	0.30	0.04
Dead time correction	-0.11	0.08
A_I	0.64	0.04
ΔE_e	-0.05	0.02
$\Delta x, \Delta y$	-0.03	0.02
$\Delta x', \Delta y'$	0.03	0.03
Aluminum windows (H ₂ target)	0.16	0.02
Dilution from π^0 decay	0.00	0.06
P_e measurement	-1.07	0.11
P_e interpolation	0.00	0.19
Systematic error		0.26

contribution is possible by comparing the measured physics asymmetry A_{phys} with the averaged theoretical value without strangeness contribution to the vector form factors A_0 . The difference $A_{\text{phys}} - A_0$ is proportional to an averaged combination of the Sachs form factors and the extracted value is $G_E^s + 0.225G_M^s = 0.039 \pm 0.034$. If one uses the Dirac and Pauli form factors instead, the extracted value is $F_1^s + 0.130F_2^s = 0.032 \pm 0.028$. The solid line in Fig. 3 illustrates the possible combinations of G_E^s and G_M^s given by our result on the measured combination of $G_E^s + 0.225G_M^s$ at $Q^2 = 0.230 \text{ (GeV/c)}^2$. The hatched area represents the error on $G_E^s + 0.225G_M^s$. The measured combination is small and is 1.2 standard deviations away from zero, which clearly rules out the pole fit type of theoretical models on the strangeness in the nucleon [21, 22]. From the published result on the measured asymmetry of the HAPPEX collaboration [6] at $Q^2=0.477 \text{ (GeV/c)}^2$ and $\theta_e = 12.3^\circ$, we recalculated the combination using our parametrization for the electro-magnetic form factors [11] and yield $G_E^s + 0.395G_M^s = 0.034 \pm 0.026$ and $F_1^s + 0.186F_2^s = 0.024 \pm 0.019$. In lack of more detailed information we make the ad hoc assumption, that F_2^s in the Q^2 -range between 0.1 (GeV/c)^2 and 0.5 (GeV/c)^2 can be approximated by $F_2^s = -0.150 \pm 0.150$, corresponding to $G_M^s = -0.099 \pm 0.154$. This assumption is guided by the fact that this value covers within two standard deviations all theoretical estimates as well as the SAMPLE result from [5]. This yields a value for G_E^s evaluated from our measurement of $G_E^s(Q^2 = 0.230 \text{ (GeV/c)}^2) = 0.061 \pm 0.035$ and $F_1^s(Q^2 = 0.230 \text{ (GeV/c)}^2) = 0.052 \pm 0.034$. If one makes the further approximation of neglecting the Q^2 -dependence in G_E^s , we can combine our result with the recalculated HAPPEX result by calculating the weighted average and yield an estimate of $F_1^s(0.1 \text{ (GeV/c)}^2 < Q^2 < 0.5 \text{ (GeV/c)}^2) = 0.052 \pm 0.024$ and $G_E^s(0.1 \text{ (GeV/c)}^2 < Q^2 < 0.5 \text{ (GeV/c)}^2) = 0.066 \pm 0.026$. The significance level of 2.2σ for F_1^s and 2.5σ for G_E^s which we reach using the assumption described above, leads us to the conclusion, that the combination of our measurements pre-

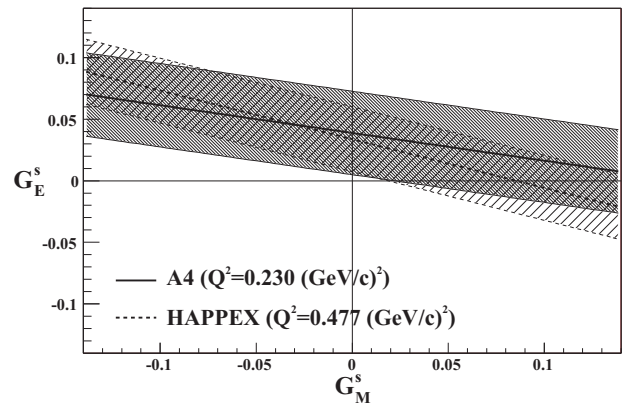


FIG. 3: The solid line represents all possible combinations of $G_E^s + 0.225G_M^s$ as extracted from the work presented here at a Q^2 of 0.230 (GeV/c)^2 . The densely hatched region represents the uncertainty. The recalculated result from the HAPPEX published asymmetry at Q^2 of 0.477 (GeV/c)^2 is indicated by the dashed line, the less densely hatched area represents the associated error of the HAPPEX result.

sented here with the earlier work of the HAPPEX collaboration shows for the first time evidence for the observation of a contribution of the strange quarks to the electric vector form factor of the nucleon.

This work is supported by the Deutsche Forschungsgemeinschaft in the framework of the SFB 201, SPP 1034, by the IN2P3 of CNRS and in part by the US Department of Energy. We are indebted to K.H. Kaiser and the whole MAMI crew for their tireless effort to provide us with good electron beam. We also would like to thank the A1 Collaboration for the use of the Møller polarimeter.

* corresponding author: maas@kph.uni-mainz.de

- [1] M. G. Olsson et al., PiN Newslett. **16**, 382 (2002).
- [2] D. Adams et al., Phys. Rev. D **56**, 5330 (1997).
- [3] D. H. Beck and B. R. Holstein, Int. J. Mod. Phys. E **10**, 1 (2001).
- [4] A. Silva et al., Nucl. Phys. A **721**, 417 (2003).
- [5] R. Hasty et al., Science **290**, 2117 (2000).
- [6] K. A. Aniol et al., Phys. Lett. B **509**, 211 (2001).
- [7] H. Euteneuer et al., Proc of the EPAC 1994 **1**, 506 (1994).
- [8] H. Weigel et al., Phys. Lett. B **353**, 20 (1995).
- [9] D. B. Kaplan et al., Nucl. Phys. B **310**, 527 (1988).
- [10] M. Musolf et al., Phys. Rep. **239**, 1 (1994).
- [11] J. Friedrich et al., Eur. Phys. J. A **17**, 607 (2003).
- [12] W. J. Marciano and A. Sirlin, Phys. Rev. D **29**, 75 (1984).
- [13] K. Hagiwara et al., Phys. Rev. D **66**, 010001 (2002).
- [14] S.-L. Zhu et al., Phys. Rev. D **62**, 033008 (2000).
- [15] F. E. Maas et al., Eur. Phys. J. A **17**, 339 (2003).
- [16] K. Aulenbacher et al., Nucl.Ins.Meth.A **391**, 498 (1997).
- [17] M. Seidl et al., Proc. of the EPAC 2000 p. 1930 (2000).
- [18] P. Bartsch, Dissertation Mainz (2001).
- [19] F. E. Maas et al., Proc. of the ICATPP-7 (World Scientific, 2002), chap. Crystal Detectors, p. 758.

[20] P. Achenbach et al., Nucl. Instrum. Meth. A **465**, 318 (2001).

[21] R. Jaffe, Phys. Lett. B **229**, 275 (1989).

[22] H. W. Hammer et al., Phys. Lett. B **367**, 323 (1996).